

Lawrence Berkeley National Laboratory

Accelerator Tech-Applied Phys

Title

81-beam coherent combination using a programmable array generator.

Permalink

<https://escholarship.org/uc/item/6n799961>

Journal

Optics Express, 29(4)

ISSN

1094-4087

Authors

Du, Qiang
Wang, Dan
Zhou, Tong
[et al.](#)

Publication Date

2021-02-15

DOI

10.1364/oe.416499

Peer reviewed

81-beam coherent combination using a programmable array generator

QIANG DU,^{*}  DAN WANG, TONG ZHOU, DERUN LI, AND RUSSELL WILCOX

Lawrence Berkeley National Lab, 1 Cyclotron Road, Berkeley, CA 94720, USA

**QDu@lbl.gov*

Abstract: We have generated 81 independently controllable beams using a spatial light modulator and combined them on a diffractive combiner, to characterize the combiner and develop a fast phase error detection scheme. A key parameter of the diffractive combiner is measured in a new way, enabling an efficient combination when programming calibrated phases of each beam. This testbed provides a platform for development of advanced feedback phase control of high channel-count beam combination.

© 2021 Optical Society of America under the terms of the [OSA Open Access Publishing Agreement](#)

1. Introduction

Recent reports have emphasized the importance of high energy, high repetition rate ultrafast lasers for scientific applications [1]. We have been developing fiber technology to meet this need, with the goal of driving laser plasma accelerators [2]. Recent work in large mode area, temporally combined fiber lasers has demonstrated $\sim 10\text{mJ}$ per amplifier output [3]. To reach multi-Joule-level pulse energies needed for our application, 100s of outputs will have to be spatially combined, making it important to minimize the number of combining optics. Currently, ultrafast, high power pulse combination uses binary trees of 2-way combiners, or splitter arrays [4]. High channel-count, tiled-aperture coherent combining has been reported [5] with $\sim 50\%$ efficiency, however close-packed tiled aperture combining has an intrinsic 67% theoretical limit. High average power CW combination can be done using a single diffractive optical element (DOE) [6], but this scheme incurs efficiency-limiting angular dispersion if broadband pulses are used.

We recently demonstrated a two-diffractive-element scheme which compensates or minimizes dispersions, combining eight 120fs pulses with no pulse distortion [7–9]. We also stabilized combining efficiency against perturbations using a new algorithm based on pattern recognition, sensing the uncombined beam intensities on a camera as data [10]. To show how this stabilization algorithm scales to realistic numbers of beams it would be possible to simply expand the 8-beam experiment by assembling a large array of phase shifters, collimators and mirrors, but this would be cumbersome and expensive. Instead, we chose to generate a controllable beam array more simply and input this into a larger channel-number diffractive splitter, creating a convenient platform for algorithm development.

We chose a commercial off-the-shelf diffractive splitter instead of designing our own DOE, to show that this characterization and control method is generic, not specific to a specially designed combining element, and is suitable for any diffractive coherent beam combining analysis. In the case of a specially designed DOE, this measurement method can be a way of experimental verification against fabrication errors.

For coherent beam combining, a widely used method of phase error measurement is interferometric technique [5,11], which uses an expanded reference beam to generate interferograms for each channel. The phase error measurement accuracy is limited by the number of pixels per fringe and camera dynamic range. In comparison, our method does not require a reference beam,

is not subject to fringe limitation, the characterization only needs to be done using one optical element (Spatial Light Modulator, SLM), and is fully programmable and reproducible. The physical model built upon this method could be then used for feedback algorithm developments.

2. Beam array formation using a spatial light modulator

Having previously shown that the diffractive optic pair works with short pulses, we used a CW signal instead, with no change to the combining principle. 81 beams were formed and controlled using a spatial light modulator (Hamamatsu X13138–02) as shown in Fig. 1.

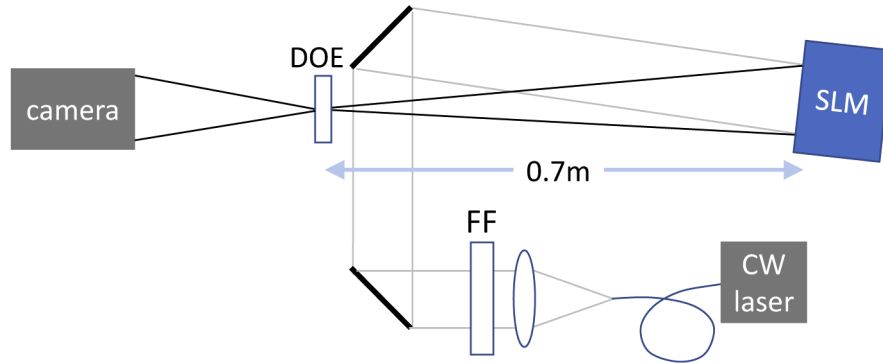


Fig. 1. SLM combiner experiment. DOE: diffractive optical element. FF: beam intensity flattening filter.

A CW source produces a beam which is collimated, flattened using a Gaussian ND filter, then sent to the SLM at near normal incidence. The SLM is a programmable phase hologram (in this case, a set of blazed gratings diffracting light into the first order), enabling control over all beam parameters except polarization; location, size, intensity profile, two directions of angle, amplitude and phase, as listed in Table 1. It is possible to move the grating lines parallel to their spacing in sub-period increments, which varies the phase of the diffracted beam dynamically, enabling control of each beam. The CW beam at 1030 nm illuminates the entire SLM area of 1272×1024 pixels, where smaller zones diffract light to produce 81 independent beams, which converge on the 9×9 diffractive splitter (MS-259 from Holo/Or). The resultant 2D fan of beams is captured by a lens and a camera (Teledyne Dalsa Genie Nano M1280 NIR). The camera has an OnSemi Python1300 P1 (1.3M) sensor without gamma corrections, and the response is linear with respect to the number of photons received by the sensor. Camera is configured with Mono 10-bit pixel format readout through Ethernet at 30 frames per second, at a fixed exposure time without analog gain (39.7 dB SNR), so the sensor sensitivity is constant. In this way, we can form a 9×9 array of independently controlled beams without difficulty.

Table 1. Each beam has independent control of parameters in beam array formation

Beam Parameter	Hologram control
Tilt Angle in x	Modulation spatial frequency in x
Tilt Angle in y	Modulation spatial frequency in y
Position in x	Centroid location in x
Position in y	Centroid location in y
Transverse Profile	Modulation depth function
Amplitude	Modulation depth mean value
Phase	Modulation offset

The generation of an input beam array can be updated at up to 60 Hz. The parameters are calculated using the inverse 2D Fourier transform and experimentally optimized to form a cone of beams converging at the DOE plane. We choose a circular flat-top transverse beam profile for best diffraction efficiency and beam separation, versus a square or Gaussian profile.

Figure 2 is an example of the generated hologram for 81 converging beams with balanced amplitudes, compensating uneven input beam power caused by variations in SLM efficiency as a function of horizontal diffraction angle.

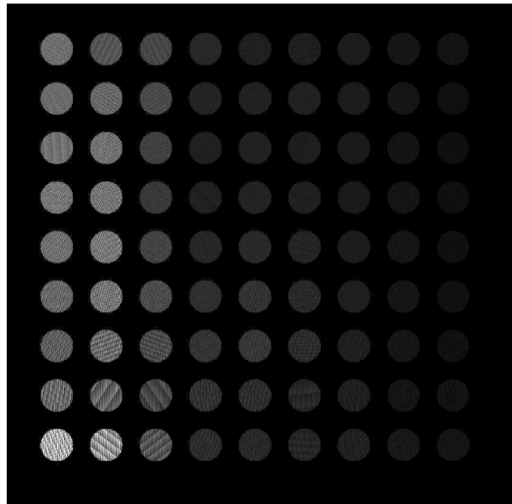


Fig. 2. Hologram on SLM for generating 9×9 beams. Gray level corresponds to grating modulation depth.

At the output, a camera images the beam pattern emerging from the DOE. For $N \times N$ input beams and a $N \times N$ shaped $d(i, j)$, there will be $(2N - 1) \times (2N - 1)$ outputs, because each input beam produces 9×9 outputs, always overlapped at the center beam. The beam size on the camera is of approximately 22 pixels in diameter.

Since the beams are formed by diffraction from programmed phase gratings, there must be enough pixels per grating line, and enough lines per beam, to achieve adequate diffraction efficiency. Also, as the number of pixels per line pair diminishes, aliasing in the digital image produces spurious higher order beams which can interfere with the wanted beams. The SLM pixel pitch is $12.5 \mu\text{m}$, and the smallest width is 12.8 mm. We want a square array of 9×9 beams, so each diffracting spot will be smaller than $12.8/9 = 1.4$ mm diameter. Geometry of the optical setup limits the minimum diffraction angle to about 17 mrad, but, depending on beam position, there will be an additional angle of up to 16.2 mrad to allow for the required convergence into the diffractive splitter (designed as 16.7 mrad at 1064 nm but operated here at 1030 nm). So, diffraction angles are between 17 and 33 mrad, requiring from 16 lines/mm to 32 lines/mm respectively. This provides for only 2.5 pixels per line at the higher density, which is marginal. Diffraction efficiency for the high angle side of the SLM is low, but adequate for this experiment.

3. Analysis of DOE transmission function measurement

In order to achieve efficient beam combination, the splitter DOE must be presented with an input beam array with the correct phases (the same phases produced when the DOE splits one beam into many). Here is how to experimentally get them by DOE characterization.

Consider a 2D DOE grating with a intrinsic complex transmittance

$$t(x, y) = |t(x, y)|e^{j\angle t(x, y)}$$

where $|t(x, y)|$ and $\angle t(x, y)$ are the amplitude and phase of the transmittance. Designed as a diffraction splitter, $t(x, y)$ is only non zero at certain diffraction orders, so we can express $t(x, y)$ as a discrete complex function $d(i, j)$, where i, j are integers, representing the order number in x and y axes respectively.

Then the physical process of 2D diffractive combining is known [10,12] as a 2D convolution of the discrete complex input beam function $b(i, j)$ with $d(i, j)$

$$\begin{aligned} s(i, j) &= \sum_{m=-\infty}^{\infty} \sum_{n=-\infty}^{\infty} b(i, j)d(i - m, j - n) \\ &= b(i, j) * d(i, j) \end{aligned} \quad (1)$$

where

$$i, j, m, n \in \mathbb{Z}, \quad s(i, j), b(i, j), d(i, j) \in \mathbb{C}^2$$

The resulting $s(i, j)$ is the complex amplitude of diffracted beam at far field; and (i, j) is the integer Cartesian coordinate of either input beam array or far field diffracted beam array from the incident direction, centered at the center input beam or zero order diffracted beam at $(0, 0)$. For the following discussion, the absolute phase modulation on the zero order beam, $\angle d(0, 0) = 0$, is ignored because only the relative phases between the diffracted beams are of interest for coherent combining.

We measure $d(i, j)$ in order to understand which output patterns correspond to which input phases, and to derive phase errors from output patterns. The phase of $d(i, j)$, as $\angle d(i, j)$, is typically not intentionally designed, but is the result of an automated genetic algorithm search for the highest efficiency DOE design, with phases as free parameters [13]. $\angle d(i, j)$ is a characteristic of the combining element, and can be found experimentally by correlating the intensities of output spots contributed to by only two input beams with the relative phase between those input beams. With that information, we can predict the output pattern given any set of amplitudes and phases of the inputs.

When the measurements of $d(i, j)$ are complete, we have the intrinsic phase function and can predict output patterns given any arbitrary input, as well as present the DOE with an ideally phased beam array. Optimal combining requires that all incident beams constructively add to the zeroth order diffracted beam, a phase condition which can be defined as

$$\angle b(i, j) = -\angle d(-i, -j) \quad (2)$$

which means that the DOE is presented with a beam array which matches its intrinsic phase function. When this input array is other than ideal, there will be excess loss.

The coherent combining efficiency loss as a function of equal probability, uncorrelated RMS piston phase error σ_ϕ (in radian) from each channel is $1 - \eta = \sigma_\phi^2$. [14] This is the main contribution to error we observe in practice, and the main subject of our control efforts. To achieve <1% efficiency loss requires $\sigma_\phi < 6^\circ$, which will be our stabilization goal.

We want to find the intrinsic DOE phase function $\angle d(i, j)$, now defined as $\theta(i, j)$, so we can retrieve the phase error given an output beam intensity pattern. In principle, this can be done using just 3 beams, one reference beam at (i_r, j_r) , and each one test beam displaced in x and y direction with respect to the reference. We interfere two at a time, with the reference beam in common, and vary its phase while recording the diffraction pattern $|s(i, j)|^2$, so it can be related

to the phases by

$$|s(i, j)|^2 = 2 + 2 \cos(\Delta\phi + \Delta\theta) \quad (3)$$

where $\Delta\phi$ is the relative input beam phase, and $\Delta_x\theta, \Delta_y\theta$ is the difference function of the intrinsic phase in each direction:

$$\Delta\theta = \begin{cases} \Delta_x\theta(i, j) = \theta(i, j) - \theta(i - 1, j) & \text{Horizontal} \\ \Delta_y\theta(i, j) = \theta(i, j) - \theta(i, j - 1) & \text{Vertical} \end{cases}$$

In practice, we can easily know the rate of phase scanning by knowing how the SLM grating lines move across the beams, but the additional phase offset (which we want to find) needs to be measured against a fixed “zero” or else there is an additional arbitrary additive term. We choose this point by adjusting the phases of the reference beam and the test beams relative to the center beam, to maximize their contributions to center beam power, establishing a “zero” relevant to the optimal combining condition according to Eq. (2). Then, we scan the reference beam over several cycles (varying $\Delta\phi$), and record the sinusoidal power variations of each output beam. Fourier analysis of these power variations gives the phase scanning frequency ω_0 and an offset phase function $\Phi(i, j)$ for each case:

$$\frac{\partial \angle |s(i, j)|}{\partial \Delta\phi} = \omega_0, \quad \Delta\theta(i, j) + \Delta\phi_0 = \Phi(i, j)$$

where $\Delta\phi_0 = -\Delta\theta(-i_r, -j_r)$ is the initial relative input beam phase for each case, which is part of the “zero” condition, so that the derived $\theta(i, j)$ is independent of the selection of reference beam.

This gives the difference function of the DOE phase function $\Delta_x\theta, \Delta_y\theta$, which can be cumulatively summed across the range of beam positions to yield the estimated intrinsic DOE phase function $\hat{\theta}(i, j)$.

$$\begin{aligned} \hat{\theta}_x(i, j) &= \sum_{-B \leq i \leq B} \left(\Delta_x\theta(i, j) + \sum_{-B \leq i \leq B} \Delta_y\theta(i, 0) \right) \\ \hat{\theta}_y(i, j) &= \sum_{-B \leq j \leq B} \left(\Delta_y\theta(i, j) + \sum_{-B \leq j \leq B} \Delta_x\theta(0, j) \right) \\ \theta(\hat{i}, j) &= \frac{1}{2} \left(\hat{\theta}_x(i, j) + \hat{\theta}_y(i, j) \right), \quad B = \begin{cases} \frac{N-1}{2} & \text{if } N \text{ is odd} \\ \frac{N}{2} & \text{if } N \text{ is even} \end{cases} \end{aligned}$$

Here the starting row or column for summation can be arbitrary; we choose to start from the center and sum in both directions, so that an unlimited number of higher order beams could be included. Averaging $\hat{\theta}_x(i, j), \hat{\theta}_y(i, j)$, and possibly from more symmetric cases would improve measurement accuracy.

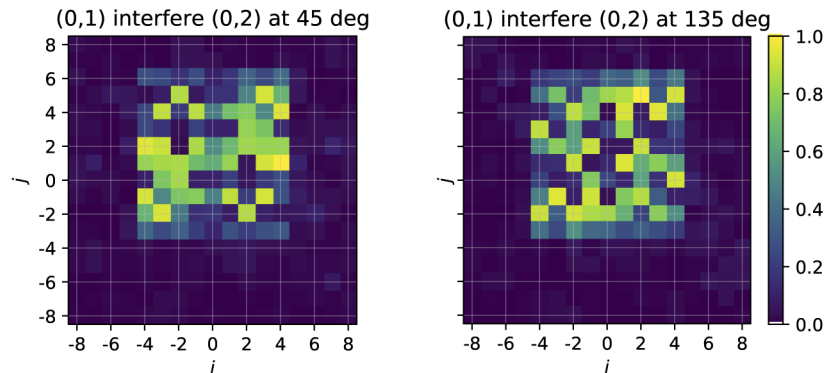
4. Experimental measurement of a DOE transmission function

The reference beam is not necessarily be the center, 0th order beam because, for our arrangement, the SLM grating lines are exactly vertical, aligned with the SLM pixels in the center row (horizontal diffraction only). The effects of aliasing, given the marginal resolution in this case, are severe for those spots. Other rows where the lines slant (vertical and horizontal diffraction together), cutting across columns of pixels, tend to average out the effects of aliasing and give much cleaner data.

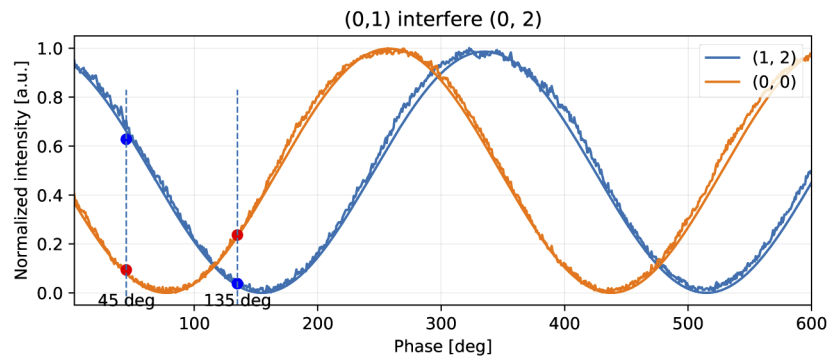
This derivation from measurement is directly analogous to the simpler case of two beam combination where an intrinsic phase offset needs to be found, if, for instance, feedback

stabilization was based on output intensity. The difference here is that we are dealing with a large matrix of beams all at once, as in Eq. (3).

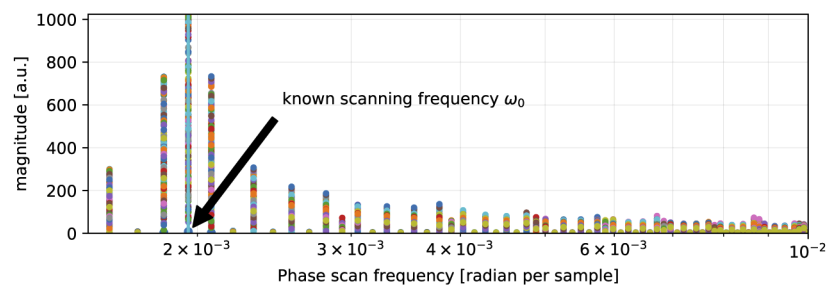
For example, when only two beams at (0, 1) and (0, 2) are enabled, and the phase of one beam is scanned, the resulting changing interference pattern is a function of the intrinsic DOE phase difference function $\Delta\theta$ and the phase difference offset of these two beams $\Delta\phi$. The phase estimation from measured sinusoidal response of the diffraction pattern function $|s(i, j)|^2$ is the summation of them, as shown in Fig. 3.



(a) Measured two-beam diffraction pattern at different beam phases Color bar unit is integrated power from camera, normalized.



(b) Measured $|s(1, 2)|^2$ and $|s(0, 0)|^2$ while scanning one beam phase



(c) Fourier magnitude response of 9×8 diffracted beams' power pattern from vertical test beam phase scanning

Fig. 3. Diffracted beam power is a function of DOE modulated beam phase, as illustrated by two-beam interference analysis

For this and all subsequent processed camera images, the axes are indices i and j , with each small square a color-mapped value of the integrated power within it. The units of plots are indicated in each caption.

Selecting input beam $(i_r, j_r) = (0, 1)$ as a reference, the vertical and horizontal DOE transmission difference phase function can be measured by analyzing interference pattern of test beam $(0, 2)$ and $(-1, 1)$ respectively, when scanning the phase of reference beam $(0, 1)$. The results are recorded as two videos of interference patterns, indexed by reference beam scanning phase. Because the phase scanning speed ω_0 is constant and common to all cases, a Fourier analysis at this frequency gives both magnitude and phase function $\Phi(i, j)$ for either horizontal or vertical test cases.

From its magnitude response as shown in Fig. 3(c), unwanted frequency components from noise and aliasing effects are filtered out, so only the phase response on the known scanning frequency ω_0 is extracted. The “zero” condition is found by tuning the test beam phase and maximizing the center combined beam $|s(0, 0)|^2$.

For both horizontal and vertical test cases, we found that using the opposite side test beam, i.e., $(0, 0)$ and $(1, 1)$ respectively, gives a negative phase function $-\Phi(i, j)$ of each phase with great accuracy, as shown in Fig. 4.

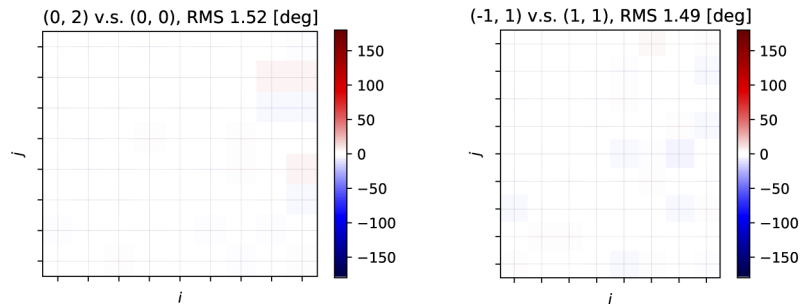


Fig. 4. Differences of Φ measured between opposite test beams. RMS estimation error is less than 1.6° . Color bar unit is degree.

We also take advantage of this over-complete set of measurements for averaging, to achieve better precision of the final DOE phase function estimation. The measured difference functions of the DOE phase function in each direction are shown in Fig. 5.

After cumulative summation in both directions, the final DOE phase function $\theta(i, j)$ is derived. A plot of the calculated $d(i, j)$ is shown in Fig. 6. The amplitude function is from a power distribution measured with only the center input beam with total power normalized to 1, so that each first order diffracted beam amplitude is approximately the DOE amplitude splitting fraction $D_n = \sqrt{1/81} = 1/9$. The measured phase function has $<1.3^\circ$ RMS error between calculations from different test beams in either horizontal or vertical cases, and $<1.9^\circ$ RMS error between $\hat{\theta}_x(i, j)$ and $\hat{\theta}_y(i, j)$. It is observed that the measured $d(i, j)$ has an approximate odd symmetry.

Because the DOE as a splitter is not ideal, there are more than 81 output beams when only one input beam is incident. Although they are relatively weak compared to the intended beams, they still contribute to the splitting or combining process. To be more accurate, our DOE characterization includes those higher order beams by measuring the DOE transmission function of 15×15 beams instead of 9×9 . This can be seen in the amplitude response plot in Fig. 6.

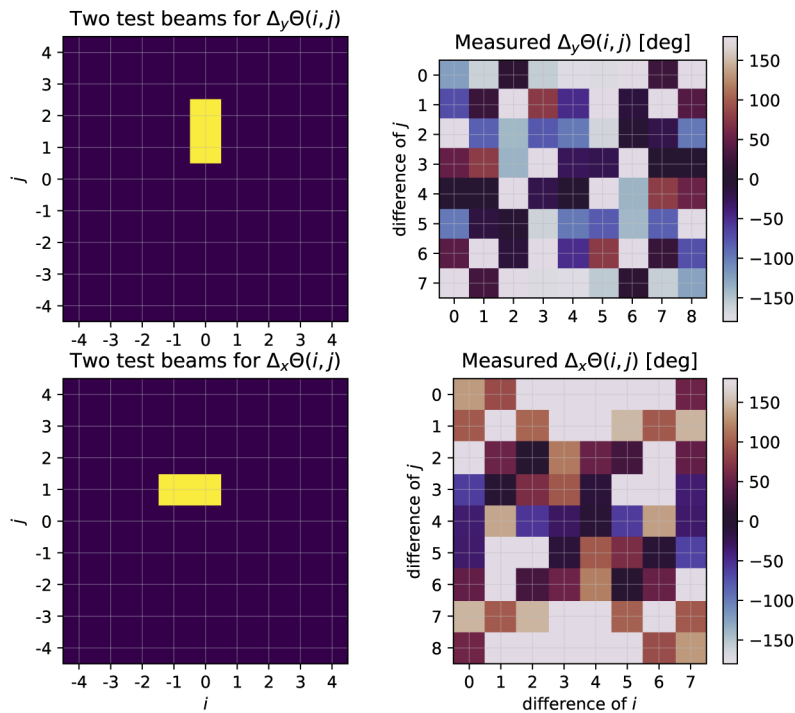


Fig. 5. Measured DOE difference phase functions in both directions. Color bar unit in phase plot is degree. Only overlapped locations in diffractive pattern are shown, resulting in 9×8 and 8×9 shape for horizontal and vertical test cases respectively.

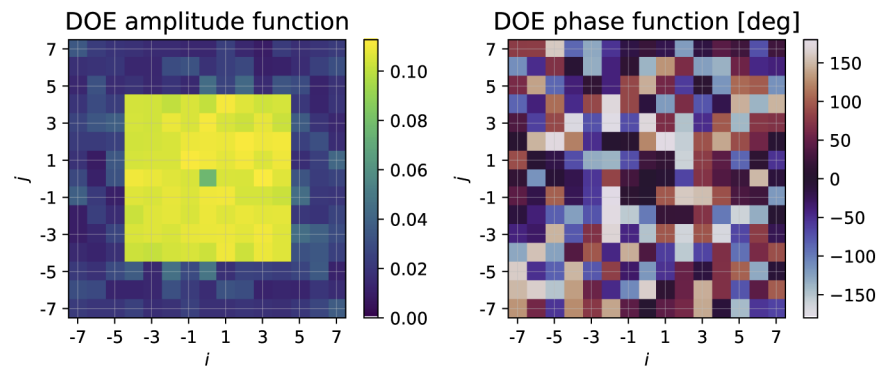


Fig. 6. Measured $d(i, j)$ of size 15×15 for a 9×9 DOE. Amplitude function is a unit-less amplitude transmission efficiency, and phase function unit is degree. The overall DOE power transmission efficiency is normalized to a lossless 100% despite uniformity.

5. Experimental combining of 81 beams

After $d(i, j)$ is characterized, it can be used to measure the actual input beam phase with respect to its SLM hologram phase shifting parameter. With the center input beam fixed as a reference, each input beam is introduced and its phase is scanned by shifting the SLM grating lines with sub-pixel resolution, so that the resulting two-beam interference pattern as a function of difference phase can be recorded. Both amplitude balancing and phase calibration can be achieved by this automated process for each input beam. As shown in Fig. 2, for a desired uniform-power input

beam array, the beam amplitude or SLM modulation depth is a function of SLM diffraction efficiency which is inversely proportional to spatial frequency (or diffraction angle), plus laser source power distribution. The input beam phase is a linear function of SLM grating line displacement, with a coefficient proportional to diffraction angle. After calibration, when the ideal beam phases described in Eq. (2) are programmed into the SLM, the coherent combination of 81 beams is achieved, resulting in a powerful center combined beam surrounded by low amplitude uncombined beams.

In order to compare the simulated and measured diffraction pattern, a linear calibration of beam power to camera sensitivity is required. We did this by introducing one input beam at a time, while measuring the combined center beam power. We found that the combined beam power is quadratic with the number of input beams as shown in Fig. 7, meaning that the power is moving from side beams to the center when adding more beams, which is what is intended.

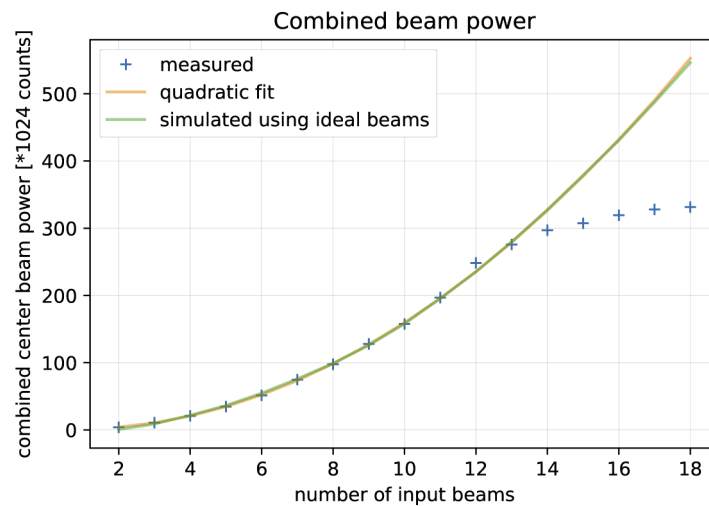


Fig. 7. Measured combined beam power when adding one beam at a time, as calibration between camera reading and simulation. Additive combined power is proportional to number of beams before the camera starts to saturate starting at 13th input beam, confirming the quadratic power increase. The quadratic polynomial fit matches well with simulated data using ideal beams after linear calibration.

In this work, we are using the camera more like a power meter, which responds to the area-integrated photocurrent irrespective of the beam size incident on the sensor. We do the same thing by integrating over an area, that covers the diffracted beam size. The power is in our special units, not the usual Watts, because we are concerned with ratios of power, not absolute measurements. We define one power unit as the power of one diffracted spot after the DOE, when one beam is incident. This will be $1/81$ of the incident beam power. When the 81 beams are optimally combined, the output power in the central beam will be 81 times the power of one input beam, and 81^2 times the power of our defined power unit. Our simulation captures the measured 5% uniformity of DOE splitting efficiency, and the 55% zero-order relative to the average, without impacting the above theoretical expectations.

The power contrast between the combined beam and the side beams increases when more beams are added, and will easily go beyond the camera's dynamic range, resulting in an incomplete measurement due to camera saturation. The data from unsaturated camera measurement is still able to provide enough information for phase corrections, as shown in a machine learning based pattern recognition method [15], where the controller only cares about the side beams' power. The required signal-to-noise ratio (SNR) of the camera, limited by the brightest side beam in the

diffraction pattern, is 29.7 dB, which is the ratio between the brightest side beam power and the lower limit of 10% of a beam power unit. We have shown that a camera noise of RMS 10% of the power unit is acceptable for the feedback to be stable [15]. Such SNR is achievable using a typical 10-bit or 12-bit pixel format camera.

We calculate an array of such integrated values on the grid, as the raw readings of the diffraction pattern, and calibrate it against theoretical values using the method described above, resulting the measured diffraction pattern $|s(x,y)|^2$, which is compared with simulation as shown in Fig. 8. The RMS noise from the 10-bit camera is ~ 0.15 in the same units.

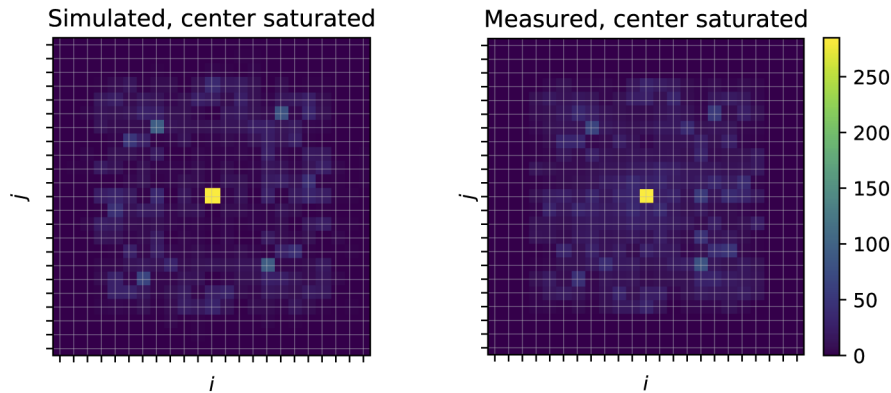


Fig. 8. Calculated and measured beam patterns for optimized 81 beam combination. Color bar unit is 1/81 of one input beam's power.

The difference between the measured and simulated patterns results from imperfect beam alignment, amplitude balancing, calibration error and noise. A difference of 8.4 RMS indicates that the derived DOE intrinsic transmittance function is accurate enough to provide a basis for further development of feedback stabilization of the combining process, as shown in Fig. 9. We found that this RMS power difference based on the 15×15 model is improved by 1.5 compared with the 9×9 (first order only) simulation result, confirming the value of including higher order beams in determining $d(i,j)$.

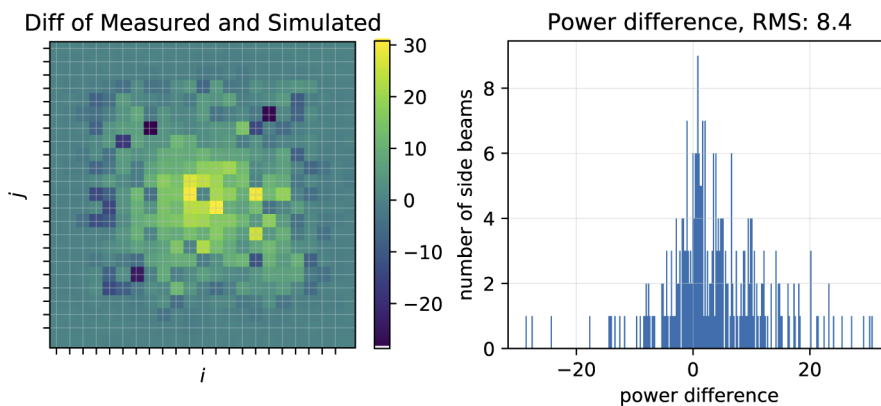


Fig. 9. Statistics of difference between simulated and measured diffraction pattern after combining 81 beams. Color bar unit is 1/81 of one input beam power.

We want to emphasize that the 2D complex transmittance function $d(i,j)$ is a complete description of the diffractive combining process, as explained in the wave superposition equations

in Leger's paper [12]. This intrinsic function is independent of experimental conditions such as overall incident beam angles and positions on the DOE. We demonstrated this when we built another test setup with different overall beam angle, beam size and position, and we found the coherent combining process is reproducible; 81 beams could be combined using the same $d(i, j)$ and combining phase condition of Eq. 2.

Figure 10 shows the full-scale simulated and measured diffraction patterns when 81 beams are combined in the new test setup. The contrast between the combined beam and the brightest side beam at $(4, -5)$ is 18.1 dB in simulation and 19.9 dB in measured data respectively. The better-than-simulation contrast may be explained by higher order beams not included in the model, similar to the previous result shown in Fig. 9. Defined as the ratio of combined center beam power to total diffracted beam power, the combining efficiency measured is 60.4%, which is reasonable compared with simulated combining efficiency of 65.3%, and given the DOE splitting efficiency (DOE-limited maximum combining efficiency) of 72%. The modeled efficiency may be less than the theoretical maximum due to our not including all the higher order diffracted beams, and other errors in measurement. We made no attempt to optimize efficiency, but will pursue this in future work.

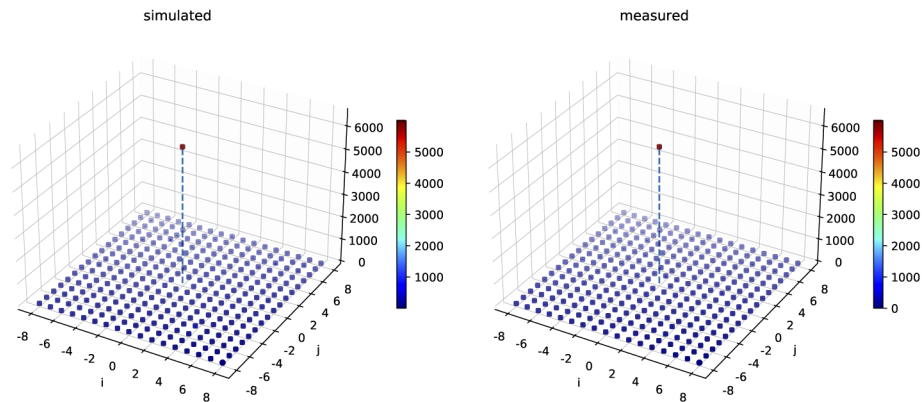


Fig. 10. Simulated diffraction pattern and raw camera image when combined. Measured data is from multiple exposure camera images to avoid saturation. Color bar unit on both plots is $1/81$ of one input beam power.

6. Conclusion

In conclusion, we have demonstrated a new way to generate a large beam array for coherent combination research, used it to characterize a diffractive element in detail, and experimentally combined 81 beams with high fidelity. This provides the basis for the phase detection scheme we are investigating using side beam pattern recognition. This demonstration shows the similarity of the coherent combining physical model to the measured result, and establishes the theoretical foundation and experimental testbed for pattern based feedback control algorithm development, including recently reported machine-learning based control [15–17]. These results are a significant step toward kHz, ultrafast pulsed laser beam combination with an arbitrarily large number of beams, for scaling to high energy.

Funding. Office of Science (DEAC02–05CH11231).

Acknowledgments. This work was supported by the Early Career Research Program of U.S. Department of Energy, and the Laboratory Directed Research and Development Program of Lawrence Berkeley National Laboratory, under U.S. Department of Energy Contract No. DE-AC02–05CH11231.

Disclosures. The authors declare no conflicts of interest.

References

1. R. Falcone, F. Albert, F. Beg, S. Glenzer, T. Ditmire, T. Spinka, and J. Zuegel, "Workshop report: Brightest light initiative," Tech. rep., OSA Headquarters, Washington, D.C, United States (2019).
2. W. Leemans, "Workshop report: Laser technology for k-bella and beyond," Tech. rep., Lawrence Berkeley National Laboratory (2017).
3. H. Pei, J. Ruppe, S. Chen, M. Sheikhsola, J. Nees, Y. Yang, R. Wilcox, W. Leemans, and A. Galvanauskas, "10mJ energy extraction from Yb-doped 85 μ m core CCC fiber using coherent pulse stacking amplification of fs pulses," in *Advanced Solid State Lasers*, (2017), pp. AW4A–4.
4. M. Müller, C. Aleshire, A. Klenke, E. Haddad, F. Légaré, A. Tünnermann, and J. Limpert, "10.4 kw coherently combined ultrafast fiber laser," *Opt. Lett.* **45**(11), 3083–3086 (2020).
5. I. Fsaifes, L. Daniault, S. Bellanger, M. Veinhard, J. Bourderionnet, C. Larat, E. Lallier, E. Durand, A. Brignon, and J.-C. Chanteloup, "Coherent beam combining of 61 femtosecond fiber amplifiers," *Opt. Express* **28**(14), 20152–20161 (2020).
6. S. M. Redmond, D. J. Ripin, X. Y. Charles, S. J. Augst, T. Y. Fan, P. A. Thielen, J. E. Rothenberg, and G. D. Goodno, "Diffractive coherent combining of a 2.5 kw fiber laser array into a 1.9 kw gaussian beam," *Opt. Lett.* **37**(14), 2832–2834 (2012).
7. R. Wilcox, "Optical pulse combiner comprising diffractive optical elements," (2019). US Patent 10, 444, 526, B2.
8. T. Zhou, T. Sano, and R. Wilcox, "Coherent combination of ultrashort pulse beams using two diffractive optics," *Opt. Lett.* **42**(21), 4422–4425 (2017).
9. T. Zhou, Q. Du, T. Sano, R. Wilcox, and W. Leemans, "Two-dimensional combination of eight ultrashort pulsed beams using a diffractive optic pair," *Opt. Lett.* **43**(14), 3269–3272 (2018).
10. Q. Du, T. Zhou, L. R. Doolittle, G. Huang, D. Li, and R. Wilcox, "Deterministic stabilization of eight-way 2d diffractive beam combining using pattern recognition," *Opt. Lett.* **44**(18), 4554–4557 (2019).
11. M. Antier, J. Bourderionnet, C. Larat, E. Lallier, E. Lenormand, J. Primot, and A. Brignon, "khz closed loop interferometric technique for coherent fiber beam combining," *IEEE J. Sel. Top. Quantum Electron.* **20**(5), 182–187 (2014).
12. J. R. Leger, G. J. Swanson, and W. B. Veldkamp, "Coherent laser addition using binary phase gratings," *Appl. Opt.* **26**(20), 4391–4399 (1987).
13. F. Wyrowski and O. Bryngdahl, "Iterative fourier-transform algorithm applied to computer holography," *J. Opt. Soc. Am. A* **5**(7), 1058–1065 (1988).
14. G. D. Goodno, C.-C. Shih, and J. E. Rothenberg, "Perturbative analysis of coherent combining efficiency with mismatched lasers," *Opt. Express* **18**(24), 25403–25414 (2010).
15. D. Wang, Q. Du, T. Zhou, D. Li, and R. Wilcox, "Stabilization of 81-channel coherent beam combination using machine learning," *Optics Express* (to be published) (2021).
16. D. Wang, Q. Du, T. Zhou, B. Mohammed, M. Kiran, D. Li, and R. Wilcox, "Artificial neural networks applied to stabilization of 81-beam coherent combining," in *2020 OSA Laser Congress*, (2020), p. ATu4A.6.
17. B. Mohammed, M. Kiran, D. Wang, Q. Du, and R. Wilcox, "Characterization and control for 81-beam diffractive coherent combining," in *2020 OSA Laser Congress*, (2020), p. JTu5A.7.